September 1986
To be published in Nucl. Instrum. Methods

BNL--39105

DE87 005244

Trace Element Measurements Using White Synchrotron Radiation

A. L. Hanson, K. W. Jones, B. M. Gordon,
J. G. Pounds, W. M. Kwiatek, and G. J. Long

Department of Applied Science
Brookhaven National Laboratory, Upton, New York 11973

M. L. Rivers and S. R. Sutton

Department of the Geophysical Sciences
The University of Chicago, Chicago, Illinois 60637

and

Brookhaven National Laboratory, Upton, New York 11973

Invited Talk, Presented at the

Ninth Conference on the
Application of Accelerators in Research and Industry

Denton, Texas
November 10-12, 1986

Trace Element Measurements Using White Synchrotron Radiation*

A. L. Hanson, K. W. Jones, B. M. Gordon,
J. G. Pounds, W. M. Kwiatek,[1] and G. J. Long[2]
Department of Applied Science
Brookhaven National Laboratory, Upton, New York 11973

M. L. Rivers and S. R. Sutton
Department of the Geophysical Sciences
The University of Chicago, Chicago, Illinois 60637
and
Brookhaven National Laboratory, Upton, New York 11973

ABSTRACT

Synchrotron radiation, when used for x-ray fluorescence (XRF) has several advantages over conventional x-ray sources. Our group at Brookhaven National Laboratory is developing the equipment and expertise to make XRF measurements with synchrotron radiation. The apparatus is briefly described, along with the alignment techniques. Some minimum detectable limits for trace elements in thin biological standards measured with white light irradiations are presented.

*Development of the X-Ray Microprobe technology supported by Processes and Techniques Branch, Division of Chemical Sciences, Office of Basic Energy Sciences, US Department of Energy Contract No. DE-AC02-76CH00016; application to biomedical problems supported by National Institutes of Health as a National Biotechnology Research Resource, Grant No. P41RR01838-03; support also received from National Science Foundation Contract No. EAR-8313682 (MLR) and National Aeronautics and Space Administration Contract No. NAG-9-106 (SRS).

[1]Permanent address: Institute of Nuclear Physics, 31-342 Krakow, Poland
[2]Permanent address: University of Arkansas for the Medical Sciences, Little Rock, Arkansas 72205

INTRODUCTION

We are presently developing and using beam line X-26C at the National Synchrotron Light Source (NSLS) for x-ray fluroescence measuremnts using synchrotron radiation (referred to as SRIXE for Synchrotron Radiation Induced X-Ray Emission). Monochromation and focussing capabilities are also being developed for this beam line and for X-26A, a beam line which will be dedicated for x-ray microprobe fluorescence (1). However, since we are presently using white light radiation for our measurements the emphasis of this paper will be on this aspect of the technique.

The advantages of using synchrotron radiation for x-ray fluorescence has been discussed in depth in previous publications (2-11). Briefly, electron synchrotron storage rings emit x-rays at brightnesses several orders of magnitude greater than conventional x-ray sources. This many-fold increase in intensity means that not only can we analyze samples faster, but we can, and many times are required to, analyze structures of the samples that are physically smaller than structures that can be analyzed with conventional x-ray fluorescence (XRF). In addition, the higher intensities of photons allows for monochromation of the beams while still maintaining usable fluxes. The intensity attribute is complemented by low beam divergences, so the x-ray beam can be brought over distances of meters while maintaining integrity of the beam. This brilliance makes focussing the beam feasible. Another attribute of particular important is the high degree of polarization of the photon beam in the plane of the electron orbit. By placing a detector at 90° to the direction of incidence, in the plane of the electron orbit, the number of x rays scattered into the detector can be minimized (12,13).

DISCLAIMER

Experimental Apparatus

A schematic of the experimental apparatus is illustrated in figure 1. The photon beam passes through a $20m$ UHV beam pipe, containing two $250\mu m$ thick Be windows. The beam size is defined with $0.8mm$ thick Ta slits mounted on four stepper-motor driven linear feedthroughs. After the beam is apertured, it passes through a helium filled ion chamber which provides the normalization of the fluorescence spectra to the incident number of photons. The (parallel) plates of this ion chamber are $8cm$ in length. Filtering of the incident photon beam occurs after the ion chamber.

Samples are mounted nominally at 45° to the beam on a stepper-motor driven stage assembly equipped with X, Y, Z, θ motion. This stage has $1\mu m$ size steps in the X,Y,Z directions. The x rays are counted with a $5mm$ thick Si(Li) detector ($145eV$ resolution at $5.9keV$) placed at 90° to the beam. The data are acquired with a LeCroy 3500 analyzer which is controlled by a DEC microVaxII computer. Data is transferred directly to the microVaxII from the LeCroy. All of the stepping motors are likewise driven with the microVaxII.

ALIGNMENT PROCEDURES

Because of the low divergence and high natural collimation of the photon beam, at $20m$ from the source most of the beam is confined within $5cm$ either side of the plane of the electron orbit (the vertical direction which is described with the angle ψ). From a line source all of the photons will be 100% polarized (electric field vectors in the plane of the electron orbit) in the mid-plane. This is illustrated in figure 2, which shows plots of the parallel, perpendicular, and total number of photons emitted into the vertical opening angle $\Delta\psi$ about the center line of the beam for several energies. These curves were calculated assuming a line source for the electron beam and integrating over increments in $\Delta\psi$ of $0.004mrad$. Figure 2 illustrates gradients, in vertical displacement for both intensity and relative polarization. Therefore in order to maintain the maximum intensities of fluorescent peaks and minimum scattering, the alignment between the beam, target and detector is important. For realistic sources the electron beam will be larger than a line (for the NSLS 4σ is on the order of $0.5mm$) so the best polarization will be on the order of 98%

Alignment is a two step process. The first step is to establish the center of the beam. There are two procedures that we regularly use. The first procedure is to set an SCA window about a high energy x ray

($> 20keV$) and slowly move a small particle producing the desired x rays through the beam while performing an MCS scan. This scan provides a vertical map of the beam flux integrated in energy over the fluorescence cross sections. Typical scans using gold, palladium and iodine are shown in figure 3. As can be seen from these scans, the spectral maps made with the higher energy photons are narrower than the maps made with the lower energy photons. This is, of course, due to the smaller opening angles for the higher energy x rays as illustrated in figure 2. These scans show raw data, and if the backgrounds were subtracted, the shapes from the spectral maps would become more apparent. The abrupt cutoffs are from fixed apertures upstream of the apparatus. The second, and simplier, procedure uses the peak to background ratio of palladium K_α peak in a fluorescence spectrum from a synthetic pyrrhotite (FeS) sample doped with $1000ppm$ palladium. If the peak to background ratio is above for 8:1, we consider the alignment to be a "good" alignment. Sample spectra from this standard are shown in figure 4 for the primary beam defining slits ($100x100\mu m$) centered $0, 0.15$ and $0.25cm$ from the mid plane. After the center of the beam is found, a general alignment of the appropriate angles between the orbit plane, detector, sample stage, and viewing system is established. For this general alignment we use diffraction spots of white light by a $< 111 >$ oriented single crystal of silicon, as described by Sutton, et al. (14). The peak to background ratio of the palladium in pyrrhotite is checked on a periodic basis to assure proper alignment of the beam has been maintained.

MDL'S

When using white light for x- ray fluorescence, the spectrum of the photon beam as it strikes the target is important since it not only fluoresces the target atoms, but the photon scatter reproduces the incudent spectrum of the beam, shifted in energy by the Compton scattering. Figure 5 shows a series of curves for the relative intensity of the photon beam after it has passed through several beam line components (namely two $250\mu m$ Be windows; $61cm$ of Helium; and $13cm$ of air, since all of our measurements are presently in air) followed by aluminum filters. The purpose of using filters is to help reduce the amount of low energy scatter and the major (or minor) element fluorescence. This reduces the total count rate that the detectors must process, while hopefully not significantly reducing the number of fluorescent x rays of interest. Superimposed on these spectra are the cross sections (from 15) for the fluorescence of the lead L_α, iron K_α, zinc K_α and calcium K_α x-rays. As can be seen from these plots the effects of the aluminum filters are not only to reduce the number of scattered low energy photons, but also to reduce the number of photons at energies that most efficiently fluoresce the atoms of interest. Therefore we have a trade-off between a reduction in background and a loss of fluorescent x-rays.

As long as the fluorescent yield does not fall off faster than the square of the scattered radiation under the peak, there will be a net improvement in the minimum detectable limits (MDL's). Figure 6 is a plot of calculated relative MDL's for calcium, iron, zinc, and lead as a function of Al absorber thickness. These relative fluorescent yields were calculated by integrating over energy the fluorescence cross section weighted by the incident spectra (figure 5). The background is then assumed to be equal to the incident spectra scattered (from a point source) into the energy of the characteristic x ray, assuming 98% polarization, plus contributions from incomplete charge collection. The lighter elements are more susceptible to the filtering, and therefore reach a minimum in the curve relatively rapidly. As we get out to lead (fluorescence of the Pb L_α as opposed to the K_α lines of the calcium, iron, and zinc), the minima is not easily reached and according to these simple predictions we are continually improving the situation.

Figure 7 are the results from measuring relative MDL's of iron, zinc, and lead from a thin section of mouse liver cortex. The relative MDL's are simply the square root of the background divided by the peak area. The MDL for iron clearly becomes poorer as more aluminum filters are added. For zinc there is only

a mild improvement in the MDL's with moderate filtering and for lead, the MDL's must be considered flat. Comparing with figure 6, the calculated MDL's to be more optimistic, which could be due to an alignment that is not optimum, or polarization of the photon beam is poorer than was assumed for the calculations.

The idea of continually improving MDL's, with increasing absorber thickness (as is the prediction for lead) does not necessarily mean a substantial improvement in the analysis of lead since the fluorescence yield is continually decreasing. Figure 8 is the relative number of x rays in the fluorescence peak corresponding to the data presented in figure 6. This plot illustrates a substantial drop in the yield of the fluorescence peak, and thus poorer counting statistics as a function of absorber thickness.

We have prepared some thin organic standards by dissolving 10*ppm* V, Fe, Zn, Pb, Br, Sr, and Cd in undialized gelatin (20% gealtin, J.T. Baker, 5% glicerol, 75% water). The samples were then sliced with a cryomicrotome to 30μm thickness, mounted on 7μm polyimide film, then freeze-dired. Figure 9 shows spectra of the gelatin standard containing no overlapping peaks. The blank gelatin contains K, Ca, and about 1 ppm Fe, Ni, Zn and Sr. The measured MDL's for the spiked elements are shown in table 1. Also shown on this table are the measured MDL's from NIES-CRM-1 Pepperbush and NIES-CRM-5 Hair Standards.

DISCUSSION

The MDL's reported in table I include all the parameters that should be necessary to determine what is expected for a given (similar) measurement. Our experience to date is that the measurement many times determines the maximum beam spot size that will be used. A comparison with previously reported values for MDL's is not always easy since many of the parameters of the measurements were not included. Many variables affect the measurements, which include: 1.) White light vs. monochromated light. (With white light we increase the background from scattered ratiation, and with monochromatic we reduce the number of x rays available for fluorescence.) 2.) When using monochromated light, what is the band pass ($\Delta E/E$) of the monochromator, since the band pass limits the flux. 3.) With monochromated light, what is the relation between the energy of the monochromated x rays and the fluorescence edge of the element(s) of interest. Using energies at the absorption edges of the maximize fluorescence, but the Compton scattered photons interfere with the fluorescence peaks increasing the background. The energy difference between the Compton scatter peak and the Rayleigh peak becomes more pronounced with higher photon energies, so the Compton scatter peak causes more interferences when using with higher energy photons. 4.) The size of the beam spot. 5.) With white light, the composition and thickness of the primary beam filter alters the incident spectra and therefore the spectra of the scattered radiation. 6.) The composition and thickness of the matrix determine not only the background due to scatter, but thicker matricies can cause substantial attenuation of the fluoresced photons. 7.) The total number of photons, and their spectra, that strike the sample determine not only the number of fluorescent events, but will also determine the number of scatter events.

The relative MDL's shown in figures 6 and 7 were calculated and measured assuming the same beam size. This is in contrast to the measurements reproted by Iida, et al., (16) and Knochel, et al., (8,9) both of whom increased the beam aperture size as thicker filters were added in order to regain the intensity of the beam that was lost due to the attenuation of the beam. By reporting the results in this way MDL's expressed in ppm may be lowered, but when expressed in picograms the MDL's will go up. As an example Iida et al., measured metals on chelated resins and analyzing with 0 and 280 μm thick aluminum filters. For zinc they measured MDL's of 550*ppb* and 170*ppb* for the two filters, respectively. However to achieve this

their irradiation area was increased from $0.35x10^{-2}mm^2$ to $2.8x10^{-2}mm^2$. The MDL in absolute number of zinc atoms that can be fluoresced went from $0.13pg$ to $0.34pg$. Knöchel, et al., used filters between 0 and $8mm$ thick aluminum. They did not mention the beam sizes used, but did mention that they increased the beam aperture size to account for the loss in beam intensity.

It is our suggestion that the field adopts reporting the experimental parameters listed in this paper when presenting data in order to make results more understandable to potential users.

REFERENCES

1. B.M. Gordon and K.W. Jones, "Design Criteria and Sensitivity Calculations for Multielemental Trace Analysis at the NSLS X-Ray Microprobe", Proc. Eighth Intern. Conf. on the Appl. of Accelerators in Res. and Ind., Denton, Texas, Nov. 12-14, 1984, Nucl. Instr. Method. B10/11 (1985) 293-298.
2. V.B. Baryshev, G.N. Kulipanov and A.N. Skrinsky, "Review of X-Ray Fluorescent Analysis With Synchrotron Radiation", Nucl. Instr. Method. A246 (1986) 739-750.
3. J.R. Chen, B.M. Gordon, A.L. Hanson, K.W. Jones, H.W. Kraner, E.C.T. Chao, and J.A. Minkin, "Synchrotron X-Ray Fluorescence and Extended X-Ray Absorption Fine Structure Analysis", Scanning Electron Microscopy/1984/ IV pp/1483-1500, SEM, Inc., AMF O'Hare Chicago ,Ill.
4. R.D. Giauque, J.M. Jaklevic, and A.C. Thompson, "Trace Element Determination Using Synchrotron Radiation", Anal. Chem. (1986) 940-044.
5. A.L. Hanson, H.W. Kraner, K.W. Jones, B.M. Gordon, R.E. Mills and J.R. Chen, "Trace Element Measurements with Synchrotron Radiation", IEEE Trans. Nucl. Sci. NS-30 (1983), 1339-1342.
6. J.M. Jaklevic, R.D. Giauque, and A.C. Thompson, "Quantitative X-Ray Fluorescence Analysis Using Monochromatic Synchrotron Radiation", Proc. Eighth Intern. Conf. on the Appl. of Accelerators in Res. and Ind., Denton, Texas, Nov. 12-14, 1984, Nucl. Instr. Method. B10/11 (1985) 303-308.
7. K.W. Jones, B.M. Gordon, A.L. Hanson, J.B. Hastings, M.R. Howells, H.W. Kraner, and J.R. Chen, "Application of Synchrotron Radiation to Elemental Analysis", Presented at the Third Intern. Conf. on PIXE and its Analytical Applications, Heidelberg, FRG July 18-22 1983; Nucl. Instr. Method. B3 (1984) 225-231.

8. A. Knöchel, W. Petersen, and G. Tolkiehn, "X-Ray Fluorescence Analysis With Synchrotron Radiation", Nucl. Instr. Method. 208 (1983) 659-663.

9. A. Knöchel, W. Petersen, and G. Tolkiehn, "X-Ray Fluorescence Spectrometry With Synchrotron Radiation", Anal. Chim. Acta 173 (1985) 105-116.

10. W. Petersen, P. Ketelsen, A. Knöchel, and R. Pausch, "New Developments of X-Ray Fluorescence Analysis With Synchrotron Radiation (SYXFA)", Nucl. Instr. Method. A246 (1986) 731-735.

11. C.J. Sparks, Jr., "X-Ray Fluorescence Microprobe for Chemical Analysis", in Synchrotron Radiation Research, H. Winick and S. Doniach, eds., Plenum Publishing Corporation, New York, 1980, pp. 459-512.

12. A.L. Hanson, "The Calculation of Scattering Cross Sections for Polarized X-Rays", Nucl. Instr. Method. A243 (1986) 583-598.

13. A.L. Hanson, "Further Comments on the Integrated Scatterin Cross Sections for Polarized X-Rays", Nucl. Instr. Method. A249 (1986) 522-529.

14. S.R. Sutton, M.L. Rivers, and J.V. Smith, "Synchrotron X-Ray Fluorescence: The Diffraction Interference", Anal. Chem. (in press).

15. M.O. Krause, C.W. Nestor, Jr., C.J. Sparks, Jr., and E. Ricci, "X-Ray Fluorescence Cross Sections for K and L X Rays", ORNL-5399 (1978).

16. A. Ida, T. Matsushita, and Y. Goshi, "Synchrotron Radiation Excited X-Ray Fluorescence Using Wide Band Pass Monochromators", Nucl. Instr. Method. A235 (1985) 597-602.

Table I. MDLs measured in three biological standards.

Identification	Ti	V	Cr	Mn	Fe	Ni	Cu	Zn	Br	Sr	Cd	Pb
Gelatin*		.22			.15			.26	.58	.73	4.2	1.2
NIES-CRM-5	0.8		.17	.25	.26		.88	.32	.56			.63
NIES-CRM-1				.84	.18	.24	.24	.16				

Identification Slits (μm × μm)	Target Thickness	Beam Filter (μm Al)	Detector Filter (μm Kapton)	Aperture (mm)	Detector Distance (mm)	Counting Time (sec., live)	Ion Chamber (nA)
Gelatin* 100 × 100	30 μm (wet)	100	50	3	40	300	1.7
NIES-CRM-5 50 × 50	.25 mm	100	100	3	40	600	.5
NIES-CRM-1 50 × 50	1 mm	200	32	3	40	1900	0.09

*The MDLs are based on the wet weight which is 75% water.
The MDLs for the dry weight will be 4 times higher.

FIGURES

1. Schematic of the XRF Apparatus.
2. Spectra calculated for the NSLS at 20 meters for 10, 20, and 30 keV x rays showing the parallel, perpendicular, and total photon intensities. The calculations are for $100mA$ at $2.529GeV$ with a bandwidth of $1eV$ and is integrated over vertical opening angle increments of $0.004mrad$.
3. Vertical intensity scans made with gold, palladium, and iodine x rays.
4. Palladium K_α and K_β peaks from a sample spectra from a standard of $1000ppm$ palladium in synthetic pyrrhotite (FeS). This standard is used to assure alignment of the system by maintaining a high peak to background ratio. The three curves are for the beam defining slits centered 0, 0.15, and $0.25mm$ from the mid plane. The peak to background ratios for the palladium K_α peaks ($21.1keV$) for these three slit positions are 8.5, 7.5, and 6.2, respectively. For these spectra the Si(Li) detector was $40mm$ from the target with a $3mm$ diameter detector aperture. The detector was filtered with $175\mu m$ aluminum and the primary beam was filtered with $400\mu m$ aluminum. The beam defining slits were $100x100\mu m$.
5. The intensity of photons from the NSLS, using the same conditions from figure 1 after the beam has passed through 0, 2, 4, 6, 8, 10, 12, 16, and 24 mil Al filters. Superimposed on this graph are relative fluorescence cross sections for calcium (x), iron (□), zinc (◇), and lead (o).
6. Predicted relative MDL's as a function of aluminum filter thickness for calcium (x), iron (□), zinc (◇) and lead (o).
7. Measured relative MDL's as a function of aluminum filter thickness for iron (□), zinc (◇) and lead(o) from a thin section of a mouse liver cortex.
8. Predicted relative fluorescence as a function of aluminum filter thickness for calcium (x), iron (□), zinc (◇) and lead (o).
9. Spectra of a blank gelatin sample and a gelatin spiked with $10ppm$ each of V, Fe, Zn, Pb, Br, Sr, and Cd.

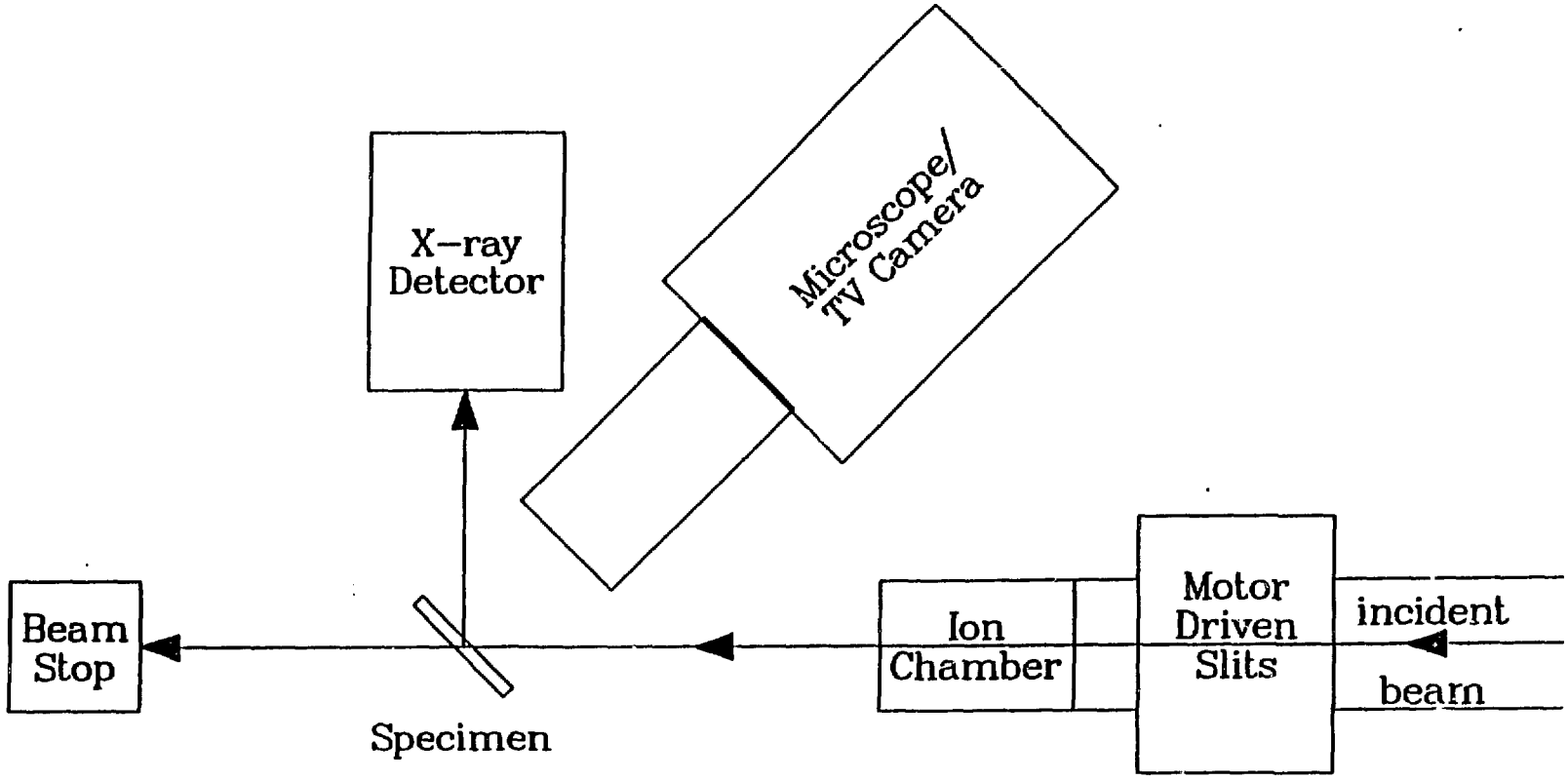

Synchrotron XRF Apparatus Schematic

Figure 1

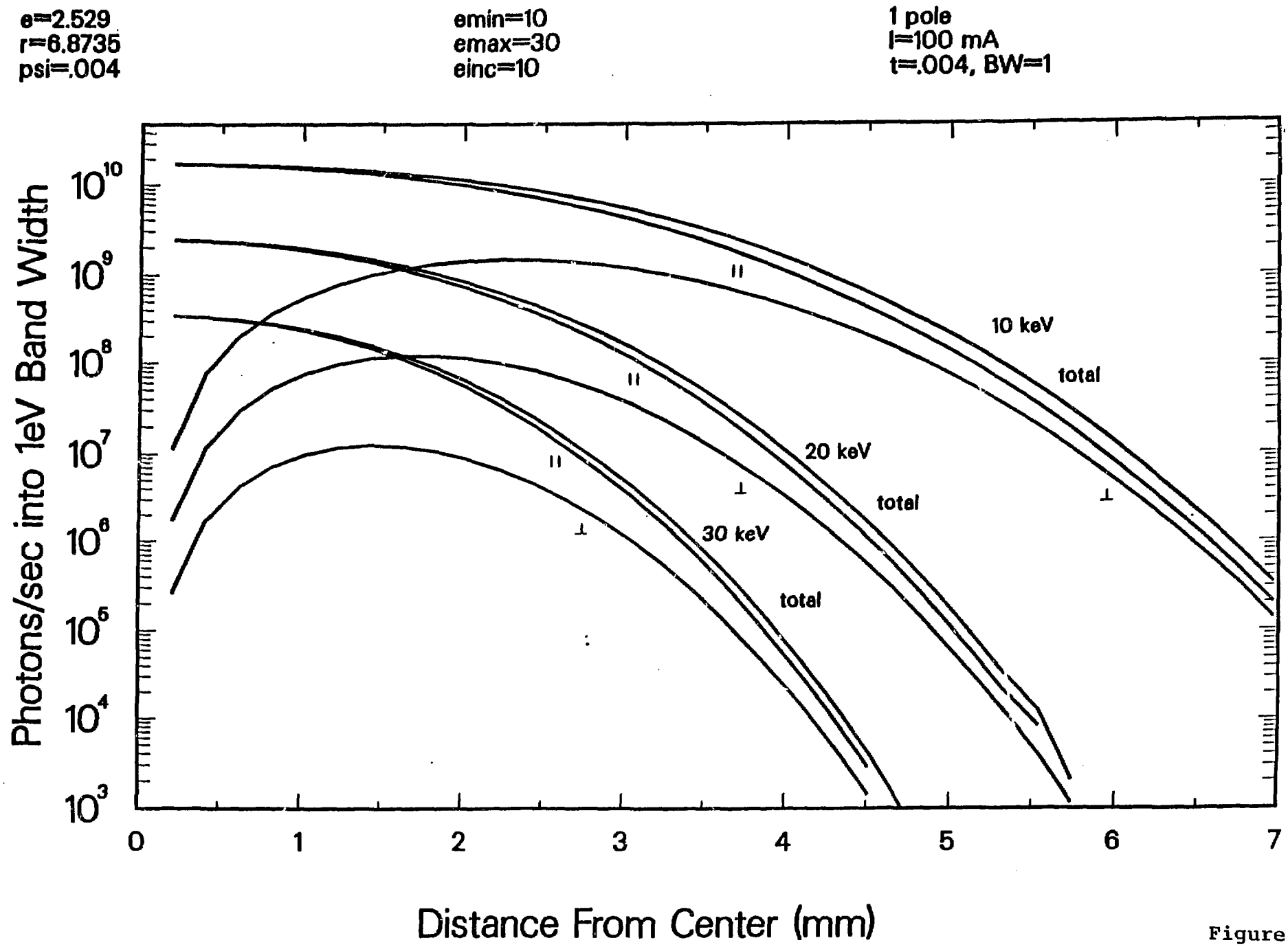
e=2.529
r=6.8735
psi=.004
emin=10
emax=30
einc=10
1 pole
I=100 mA
t=.004, BW=1
Photons/sec into 1eV Band Width
10^{10}
10^{9}
10^{8}
10^{7}
10^{6}
10^{5}
10^{4}
10^{3}
10 keV
total
20 keV
total
30 keV
total
0
1
2
3
4
5
6
7
Distance From Center (mm)

Figure 2

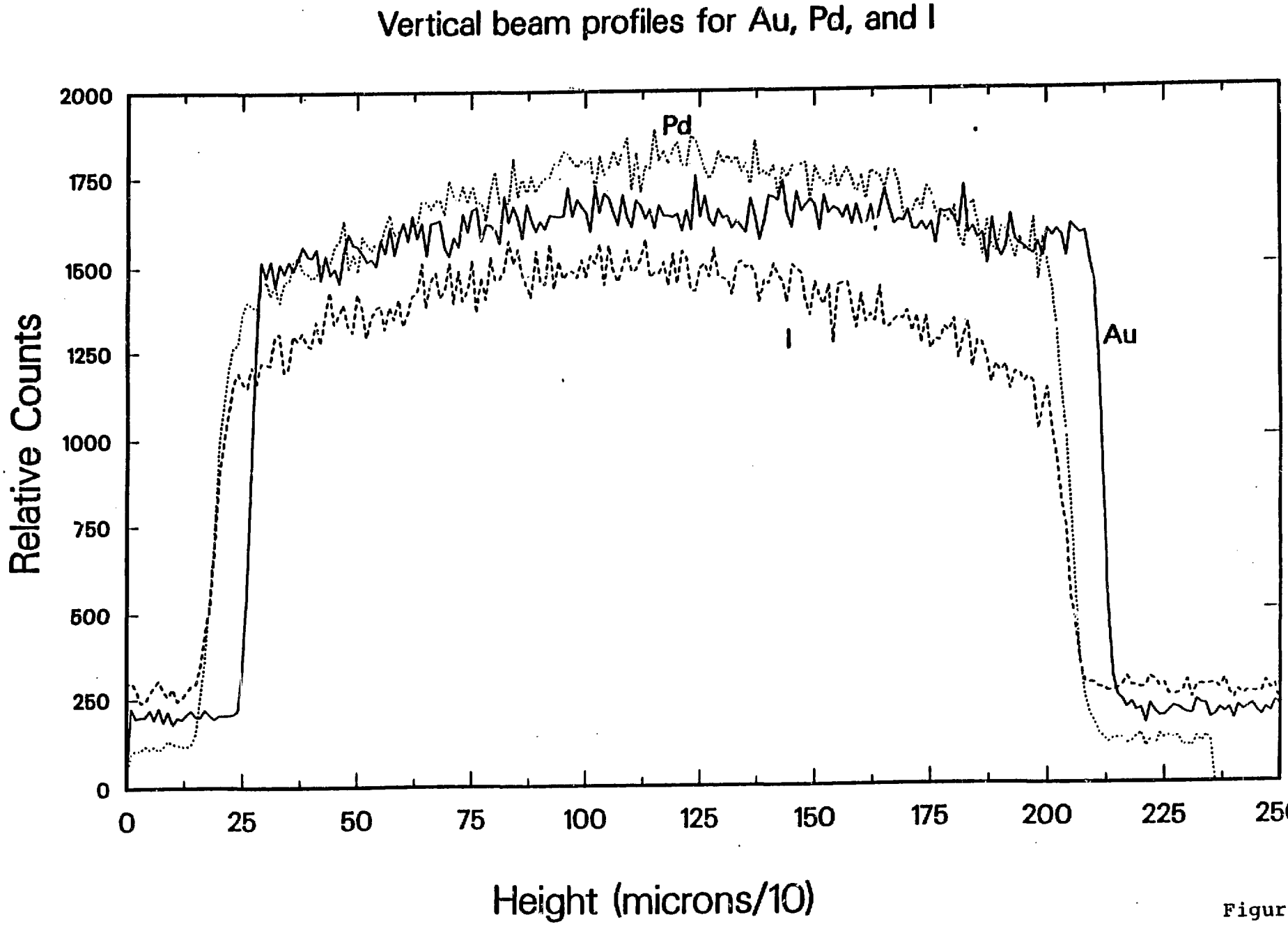
Vertical beam profiles for Au, Pd, and I
Relative Counts
Height (microns/10)
Pd
I
Au
2000
1750
1500
1250
1000
750
500
250
0
0
25
50
75
100
125
150
175
200
225
250

Figure 3

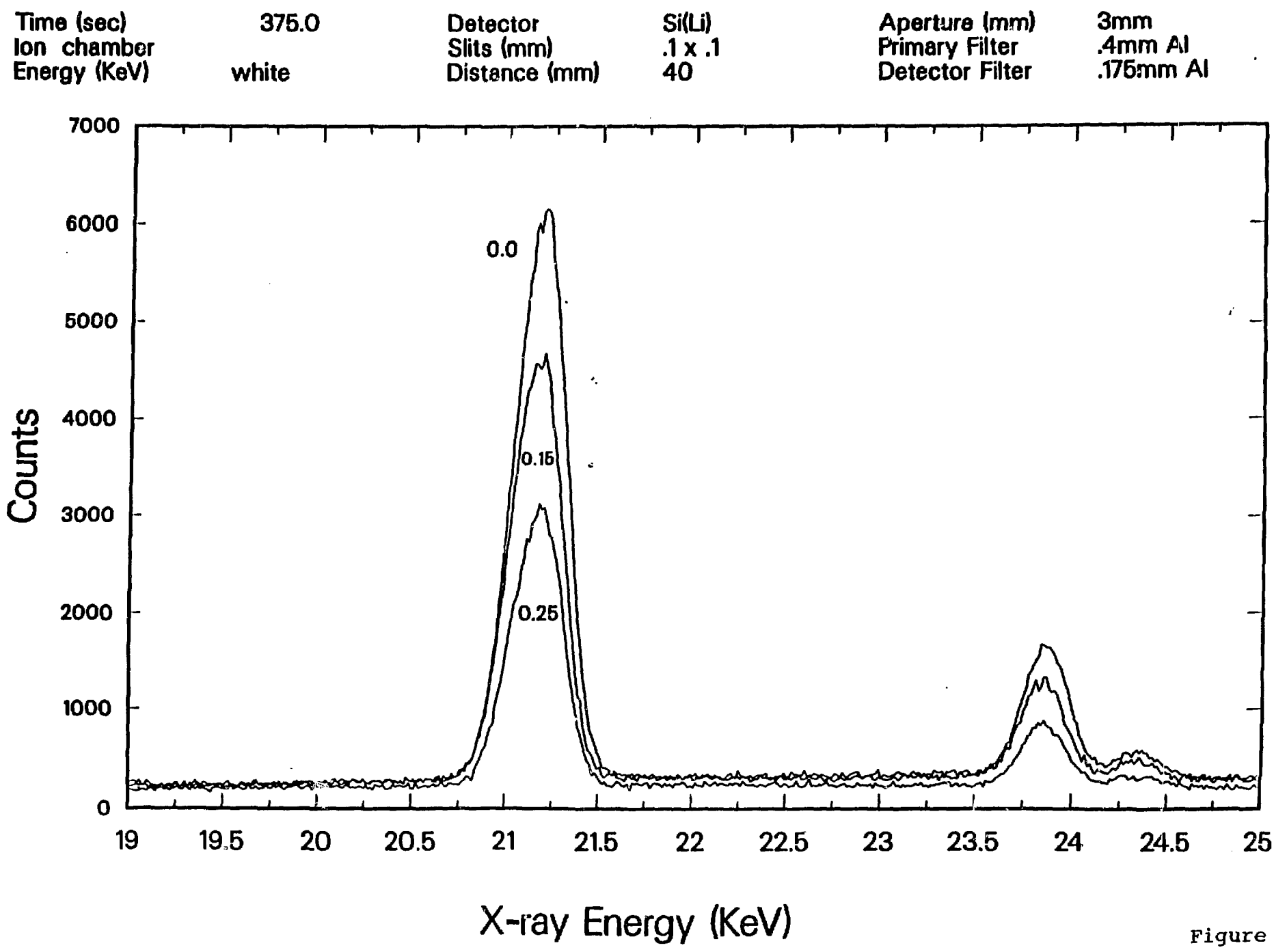
Time (sec) 375.0
Ion chamber
Energy (KeV) white
Detector Si(Li)
Slits (mm) .1 x .1
Distance (mm) 40
Aperture (mm) 3mm
Primary Filter .4mm Al
Detector Filter .175mm Al
7000
6000
5000
4000
3000
2000
1000
0
Counts
0.0
0.15
0.25
19
19.5
20
20.5
21
21.5
22
22.5
23
23.5
24
24.5
25
X-ray Energy (KeV)

Figure 4

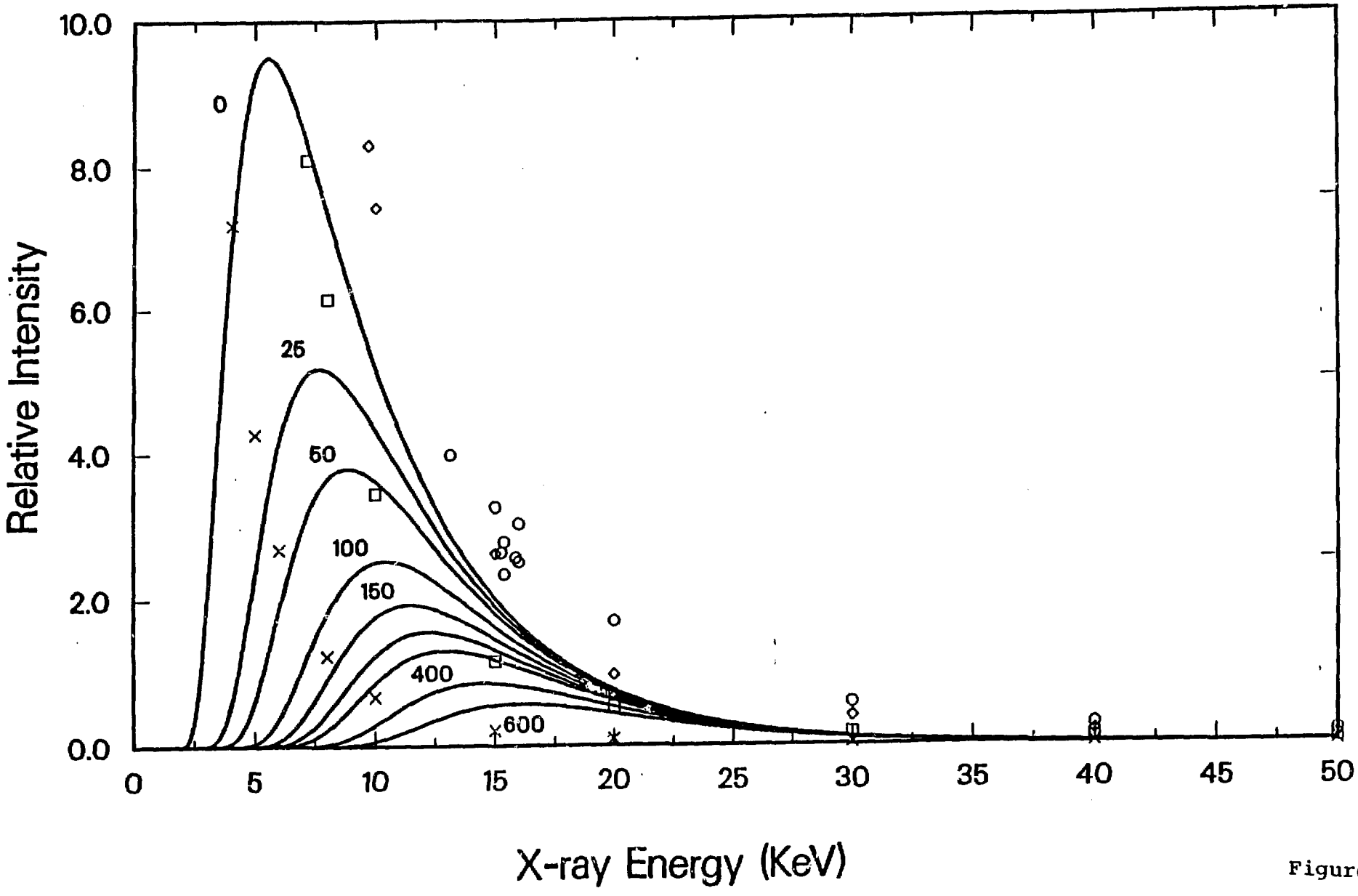
e=2.529
r=6.8735
psi=.004
emin=1
emax=50
einc=.1
1 pole
I=100 mA
t=.004, BW=1
10.0
8.0
6.0
4.0
2.0
0.0
Relative Intensity
0
25
50
100
150
400
600
0
5
10
15
20
25
30
35
40
45
50
X-ray Energy (KeV)

Figure 5

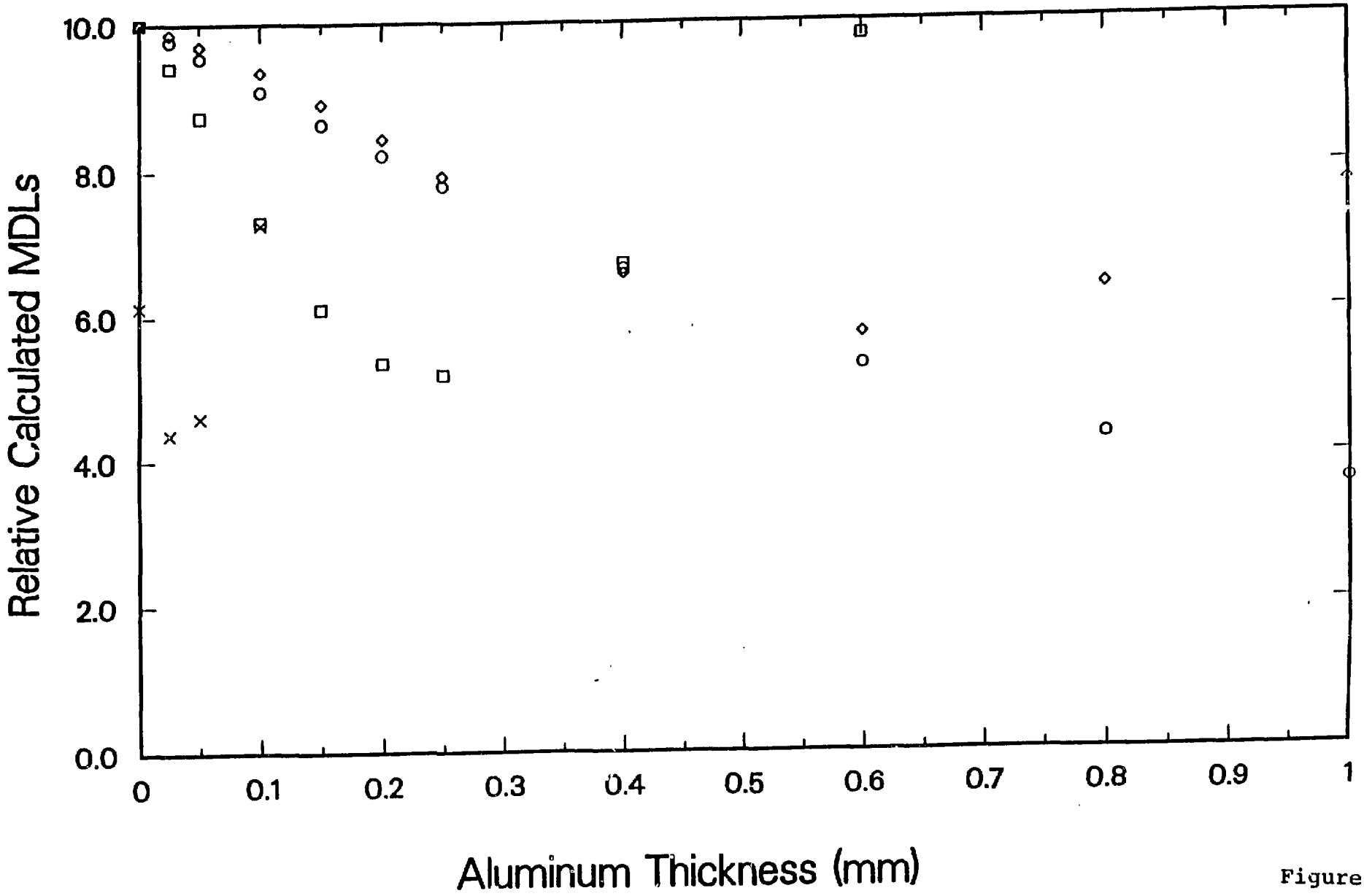
Relative Calculated MDLs
10.0
8.0
6.0
4.0
2.0
0.0
0
0.1
0.2
0.3
0.4
0.5
0.6
0.7
0.8
0.9
1
Aluminum Thickness (mm)

Figure 6

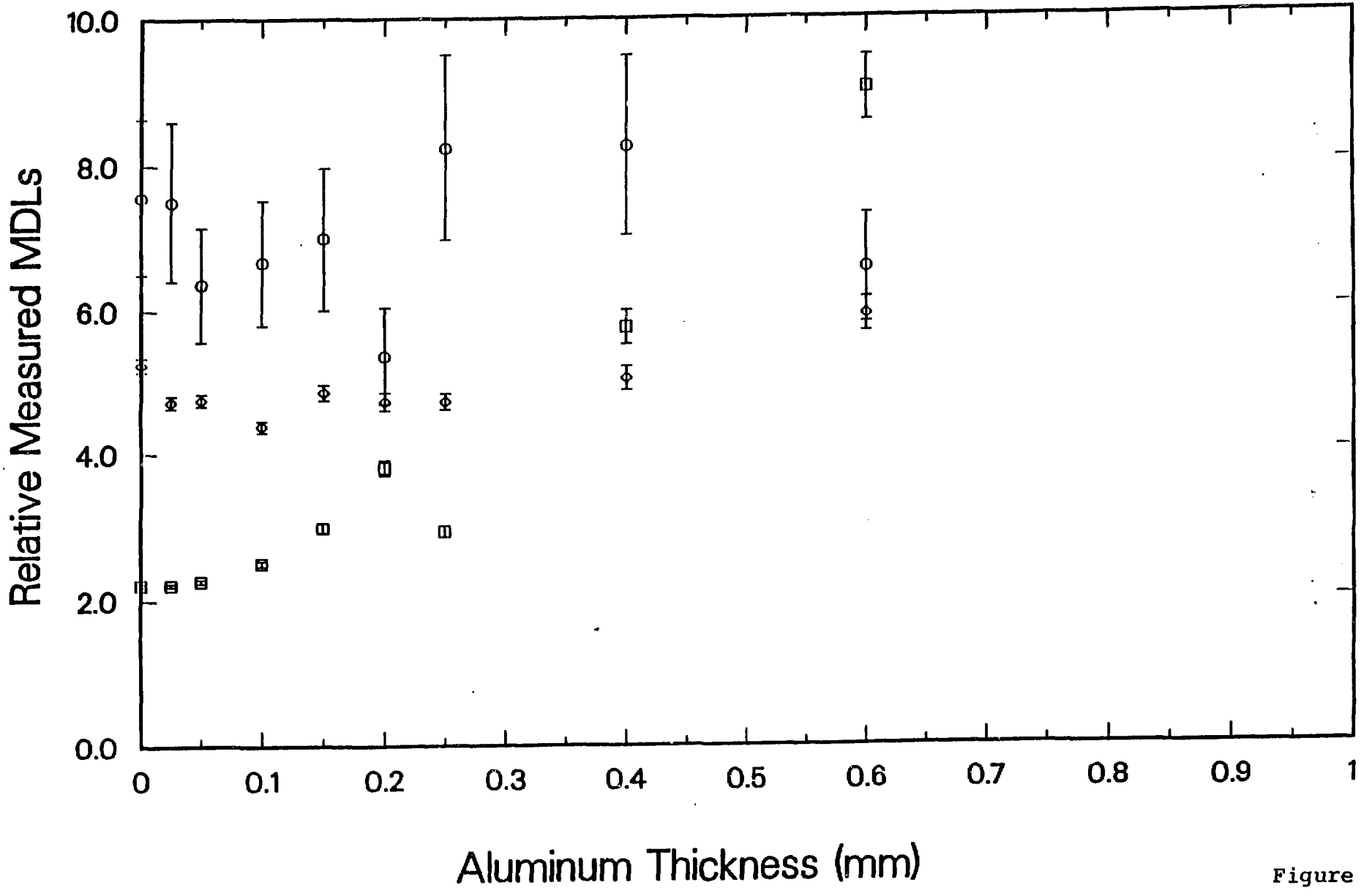
10.0
8.0
6.0
4.0
2.0
0.0
Relative Measured MDLs
0
0.1
0.2
0.3
0.4
0.5
0.6
0.7
0.8
0.9
1
Aluminum Thickness (mm)

Figure 7

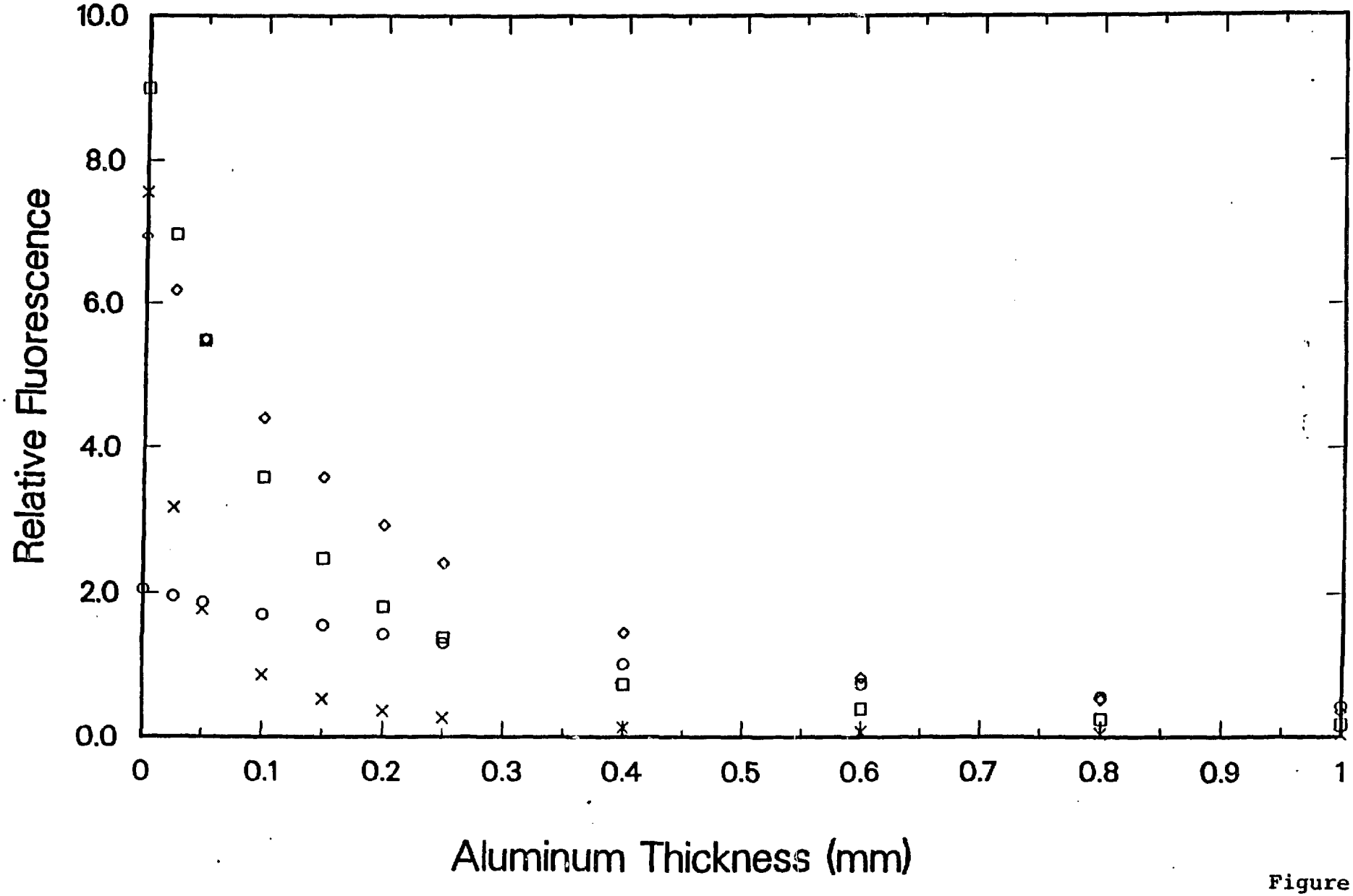
10.0
8.0
6.0
4.0
2.0
0.0
Relative Fluorescence
0
0.1
0.2
0.3
0.4
0.5
0.6
0.7
0.8
0.9
1
Aluminum Thickness (mm)

Figure 8

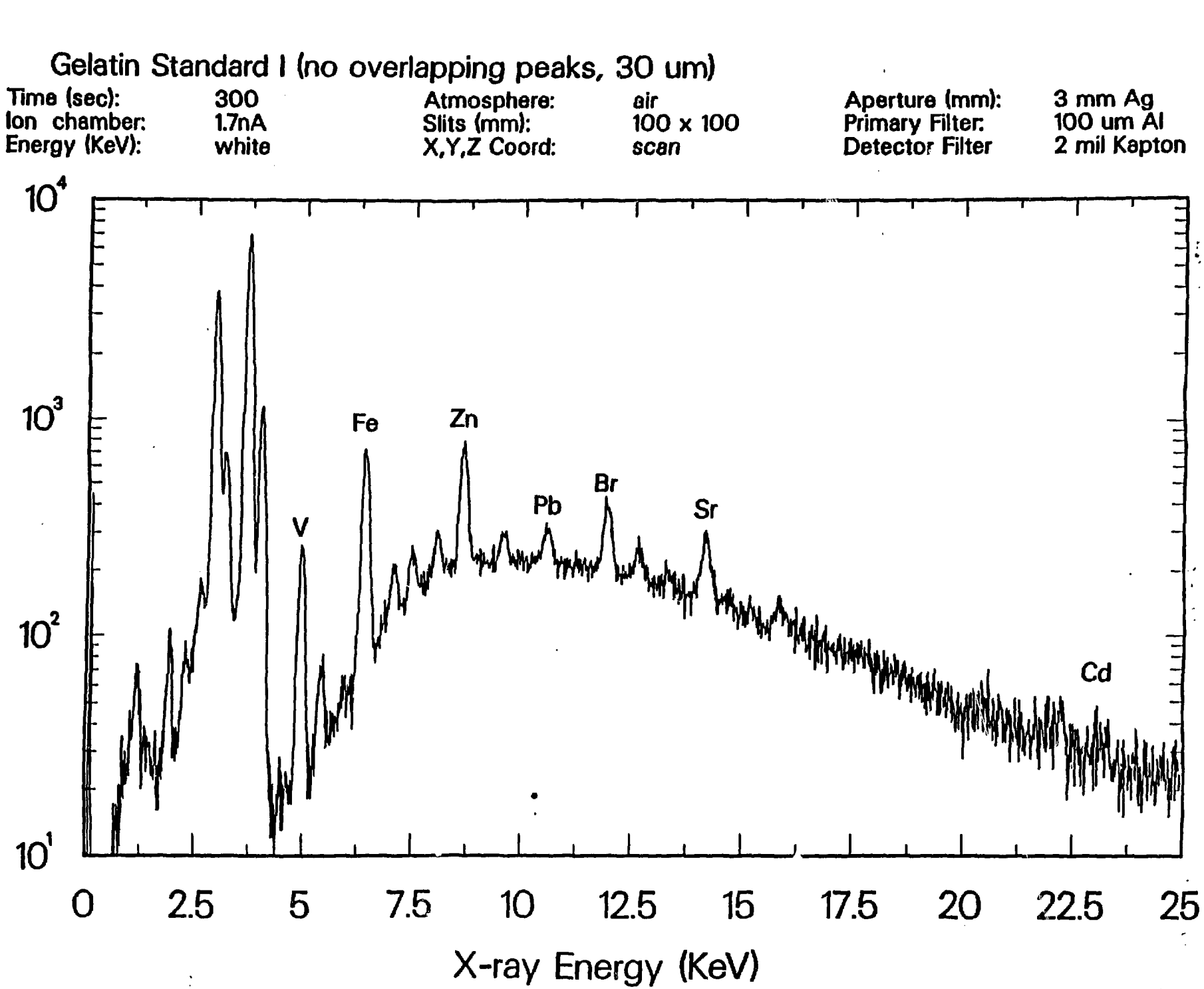
Gelatin Standard I (no overlapping peaks, 30 um)
Time (sec): 300
Ion chamber: 1.7nA
Energy (KeV): white
Atmosphere: air
Slits (mm): 100 x 100
X,Y,Z Coord: scan
Aperture (mm): 3 mm Ag
Primary Filter: 100 um Al
Detector Filter 2 mil Kapton
10^4
10^3
10^2
10^1
V
Fe
Zn
Pb
Br
Sr
Cd
0
2.5
5
7.5
10
12.5
15
17.5
20
22.5
25
X-ray Energy (KeV)

Figure 9